# Application of Artificial Neural Network State Feedback Controller to Torque Ripple Minimization of PMSM

L. Niewiara[1], T. Tarczewski[1] and L. M. Grzesiak[2]

[1]*Institute of Physics, Faculty of Physics, Astronomy and Informatics, Nicolaus Copernicus University, Grudziadzka 5, Torun, Poland*
[2]*Institute of Control and Industrial Electronics, Warsaw University of Technology, Koszykowa 75, Warsaw, Poland*

Abstract:     This paper deals with the problem of torque ripple minimization of permanent magnet synchronous motor. The novelty of the presented approach lays in precisely maintain the level of the voltage source inverter DC voltage demanded for proper operation of the motor. An additional voltage matching circuit with state feedback controller is introduced in order to control of the inverter DC voltage. In the proposed solution model of a plant (i.e. permanent magnet synchronous motor fed by voltage source inverter with additional voltage matching circuit) is non-linear and non-stationary. An adaptive state feedback controller is developed by using an artificial neural network, which approximates non-linear control gain surfaces. A simple adaptation algorithm based on 2 low-order low-pass filters is used. Simulation results illustrate the proposed approach in comparison to typical drive with voltage source inverter and stationary state feedback controller.

## 1 INTRODUCTION

Minimization of torque ripple is an important requirement in a wide range of high performance motion control applications with permanent magnet synchronous motor (PMSM) such as robots, machine tools and satellite trackers (Jahns and Soong, 1996). The torque ripple generates unwanted mechanical vibration (Gulez et al., 2008) and deteriorates performance of the drive (Hasanien, 2010).

The torque ripple minimization can be realized by using complex control techniques: preprogrammed current waveforms for harmonics cancellation (Hung and Ding, 1993), iterative learning control (Qian et al., 2004), based on complex model of PMSM adaptive control (Petrovic et al., 2000). On the other hand an additional passive filter can be used to produce sinusoidal output waveform of the inverter (Steinke, 1999), (Kojima et al., 2004), (Tarczewski and Grzesiak, 2013).

A new approach to the torque ripple minimization is proposed in this paper. An additional voltage matching circuit (VMC) with state feedback controller is used to precisely control of the voltage source inverter (VSI) DC voltage required to proper operation of the drive. A simple adaptation algorithm

is used to determine an appropriate value of DC voltage. In the proposed solution model of a plant (i.e. PMSM fed by VSI + VMC) is non-linear and non-stationary. In this field, an interesting solution can be obtained when state feedback controller is used (Tarczewski et al., 2014). Non-linear control gain surfaces obtained for state feedback controller of PMSM are implemented by using artificial neural network (ANN) thanks to its universal approximation property (Ferrari and Stengel, 2005), (Huang and Tan, 2012).

The efficacy of the torque ripple reduction and dynamic properties of the control system are confirmed in a simulation study. Dynamic properties as well as torque ripple factor calculated for proposed control system are compared with values obtained for control system with stationary state feedback controller and PMSM fed by typical VSI.

## 2 MATHEMATICAL MODEL OF THE SYSTEM

Considered control system consists of PMSM fed by a 2-level VSI extended with voltage matching circuit. An additional buck converter (figure 1) was in-

troduced to the inverter structure in order to realize VMC. Block diagram of the proposed system is presented in figure 2.
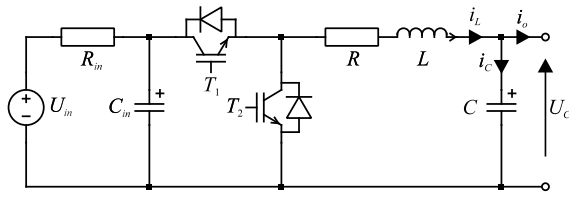


Figure 1: Topology of a buck converter.
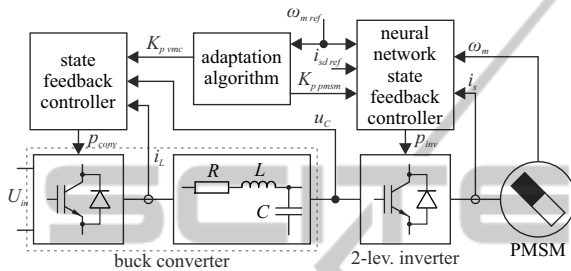


Figure 2: Block diagram of the considered control system.

## 2.1 Model of the Buck Converter

State-space model of the proposed buck converter with an output LC filter takes the following form:

$$\frac{\mathrm{d}x_b}{dt} = A_b x_b + B_b u_b + E_b d_b \qquad (1)$$

where:

$$x_b = \begin{bmatrix} i_L \\ u_C \end{bmatrix}, A_b = \begin{bmatrix} -\frac{R}{L} & -\frac{1}{L} \\ -\frac{1}{C} & 0 \end{bmatrix}, B_b = \begin{bmatrix} \frac{Kpp}{L} \\ 0 \end{bmatrix},$$

$$E_b = \begin{bmatrix} 0 \\ -\frac{1}{C} \end{bmatrix}, u_b = u_{cc}, d_b = i_o$$

$i_L$ - coil current, $u_C$ - capacitor voltage, $R$ - coil resistance, $L$ - coil inductance, $C$ - capacitor capacitance, $K_{pp}$ - buck converter gain, $u_{cc}$ - input voltage, $i_o$ - load current.

The buck converter was modeled by using proportional element. Proposed approximation is valid for sufficiency high switching frequency, omitted dead time of power transistors and linear operation area of the buck converter.

## 2.2 Model of the PMSM Fed by VSI

State-space model of the PMSM with VSI was written in an orthogonal $d$, $q$ coordinates system (Grzesiak and Tarczewski, 2011):

$$\frac{\mathrm{d}x_p}{dt} = A_p x_p + B_p u_p + E_p d_p \qquad (2)$$

where:

$$A_p = \begin{bmatrix} -\frac{R_s}{L_s} & p\omega_m & 0 \\ -p\omega_m & -\frac{R_s}{L_s} & -\frac{p\Psi_f}{L_s} \\ 0 & \frac{3p\Psi_f}{2J_m} & -\frac{B_m}{J_m} \end{bmatrix}, B_p = \begin{bmatrix} \frac{K_p}{L_s} & 0 \\ 0 & \frac{K_p}{L_s} \\ 0 & 0 \end{bmatrix},$$

$$E_p = \begin{bmatrix} 0 \\ 0 \\ -\frac{1}{J_m} \end{bmatrix}, x_p = \begin{bmatrix} i_{sd} \\ i_{sq} \\ \omega_m \end{bmatrix}, u_p = \begin{bmatrix} u_{dc} \\ u_{qc} \end{bmatrix}, d_p = T_l$$

$R_s$, $L_s$ - stator resistance and inductance, $p$ - number of pole pairs, $\omega_m$ - rotor angular speed, $\Psi_f$ - PMSM flux linkage, $J_m$ - moment of inertia, $B_m$ - viscous friction, $K_p$ - variable VSI gain, $i_{sd}$, $i_{sq}$ - space vector components of PMSM current, $u_{dc}$, $u_{qc}$ - space vector components of input voltage, $T_l$ - load torque. It should be noted that in (2) a PMSM with surface mounted magnets is taken into account. In such a case inductances in $d$ and $q$ axis are in practical equal: $L_s = L_d = L_q$. Model of PMSM presented above is non-linear and non-stationary due to the cross coupling between space vector components of the PMSM current as well as presence of the angular velocity in a state matrix $A_p$ and variable VSI gain in an input matrix $B_p$.

# 3 CONTROL STRUCTURES

## 3.1 VMC Control Structure

A discrete state-feedback controller has been used in order to precise control of the buck converter output voltage. Gain values of the controller were determined with the help of the linear-quadratic optimization method (Tewari, 2002). In order to control DC voltage without steady-state error (in a case of step variation of the reference voltage and the load current) an internal model of the reference input was introduced (Grzesiak and Tarczewski, 2013). After introduction of an internal input model and assumption that the load current is omitted an augmented state-space model is:

$$\frac{\mathrm{d}x_{bi}}{dt} = A_{bi} x_{bi} + B_{bi} u_{bi} + F_{bi} r_{bi} \qquad (3)$$

where:

$$x_{bi} = \begin{bmatrix} i_L \\ u_C \\ e_u \end{bmatrix}, A_{bi} = \begin{bmatrix} -\frac{R}{L} & -\frac{1}{L} & 0 \\ -\frac{1}{C} & 0 & 0 \\ 0 & 1 & 0 \end{bmatrix}, B_{bi} = \begin{bmatrix} \frac{Kpp}{L} \\ 0 \\ 0 \end{bmatrix},$$

$$F_{bi} = \begin{bmatrix} 0 \\ 0 \\ -1 \end{bmatrix}, u_{bi} = u_b, r_{bi} = u_{cref}$$

$u_{cref}$ - reference value of the buck converter output voltage. An additional state variable in (3) corresponds to the integral of the buck converter output voltage error:

$$e_u(t) = \int_0^t [u_c(\tau) - u_{cref}(\tau)] \, d\tau \qquad (4)$$

The following penalty matrices were used to determine gain values of the VMC controller:

$$Q_{bi} = \text{diag}\left([1 \times 10^{-3} \quad 4 \times 10^{-3} \quad 3 \times 10^3]\right), \\ R_{bi} = 1 \qquad (5)$$

Values (5) were selected empirically in order to: provide zero steady-state buck converter output voltage error for a step change of the $u_{cref}$ as well as for load current step variations; achieve maximum permissible dynamics of VMC in the linear range of modulation (at least 5 times faster than dynamics of the PMSM).

Table 1: Basic parameters of VMC.

| Parameter | Value | Unit |
|-----------|-------|------|
| $R$ | 0.1 | $\Omega$ |
| $L$ | 3 | mH |
| $C$ | 30 | $\mu$F |
| $K_{pp}$ | 600 | |

Gain coefficients of the VMC controller calculated for system (3) with basic parameters given in table 1 and for penalty matrices (5) are:

$$K_{bi} = \begin{bmatrix} 0.129 & 0.049 & 40.595 \end{bmatrix} \qquad (6)$$

## 3.2 PMSM Control Structure

Similar to VMC, control of the PMSM was realized with the help of a discrete state-feedback controller. Described type of control was chosen because of its ability to control non-stationary systems (Tarczewski et al., 2014). Note, that mathematical model of the plant (i.e. PMSM fed by VSI) would be non-stationary if VMC circuit is used. Because of presence of variable parameters in a state matrix $A_p$ and input matrix $B_p$, the dimension of non-stationarity for PMSM model (2) is 2.

As in a case of VMC control structure, an internal input models of the $d$ axis reference current and the reference angular velocity were added. An augmented state-space model of the PMSM with VSI takes the following form:

$$\frac{dx_{pi}}{dt} = A_{pi}x_{pi} + B_{pi}u_{pi} + F_{pi}r_{pi} \qquad (7)$$

where:

$$A_{pi} = \begin{bmatrix} -\frac{R_s}{L_s} & 0 & p\omega_m & 0 & 0 \\ 0 & 1 & 0 & 0 & 0 \\ -p\omega_m & 0 & -\frac{R_s}{L_s} & -\frac{p\Psi_f}{L_s} & 0 \\ 0 & 0 & \frac{3p\Psi_f}{2J_m} & -\frac{B_m}{J_m} & 0 \\ 0 & 0 & 0 & 1 & 0 \end{bmatrix}, \quad B_{pi} = \begin{bmatrix} \frac{K_p}{L_s} & 0 \\ 0 & 0 \\ 0 & \frac{K_p}{L_s} \\ 0 & 0 \\ 0 & 0 \end{bmatrix},$$

$$x_{pi} = \begin{bmatrix} i_{sd} \\ e_i \\ i_{sq} \\ \omega_m \\ e_\omega \end{bmatrix}, \quad F_{pi} = \begin{bmatrix} 0 & 0 \\ -1 & 0 \\ 0 & 0 \\ 0 & 0 \\ 0 & -1 \end{bmatrix}, \quad \begin{matrix} u_{pi} = u_p, \\ \\ r_{pi} = \begin{bmatrix} i_{sdref} \\ \omega_{mref} \end{bmatrix} \end{matrix}$$

New state variables in a state vector $x_{pi}$ (i.e. $e_i$ and $e_\omega$) correspond to the integral of the $d$ axis current and the angular velocity errors respectively:

$$e_i(t) = \int_0^t [i_{sd}(\tau) - i_{sdref}(\tau)] \, d\tau \qquad (8)$$

$$e_\omega(t) = \int_0^t [\omega_m(\tau) - \omega_{mref}(\tau)] \, d\tau \qquad (9)$$

where: $i_{sdref}$ - reference value of the $d$ axis current, $\omega_{mref}$ - reference value of the angular velocity. An internal input models presented above were introduced in order to provide zero steady-state error of the angular velocity and commonly used control strategy with zero $d$ axis current (Krishnan, 2010).

Because of non-stationarity of the model (7) gain coefficients of the state feedback controller were obtained at the operating points defined by the actual value of:

- voltage source inverter's gain $K_p \in [10; 300]$,
- PMSM's angular velocity $\omega_m \in [-314; 314]$ rad/s.

Steps of the VSI gain and PMSM angular velocity changes were chosen empirically: $\Delta K_p = 5$, $\Delta \omega_m = 2$ rad/s. Linear-quadratic optimization method was used to determine gain values of the controller (Tewari, 2002). The following penalty matrices has been chosen to determine variable gain values of the controller:

$$Q_{pi} = \text{diag}\left([q_{pi1} \; q_{pi2} \; q_{pi3} \; q_{pi4} \; q_{pi5} \; q_{pi6}]\right), \\ R_{pi} = \text{diag}\left([r_{pi1} \; r_{pi2}]\right) \qquad (10)$$

where: $q_{pi1} = 5.7 \times 10^1$, $q_{pi2} = 1 \times 10^7$, $q_{pi3} = 7.6 \times 10^{-1}$, $q_{pi4} = 1 \times 10^{-2}$, $q_{pi6} = 1.68 \times 10^2$, $r_{pi1} = r_{pi2} = 3 \times 10^{-1}$. Values (10) were selected empirically in order to:
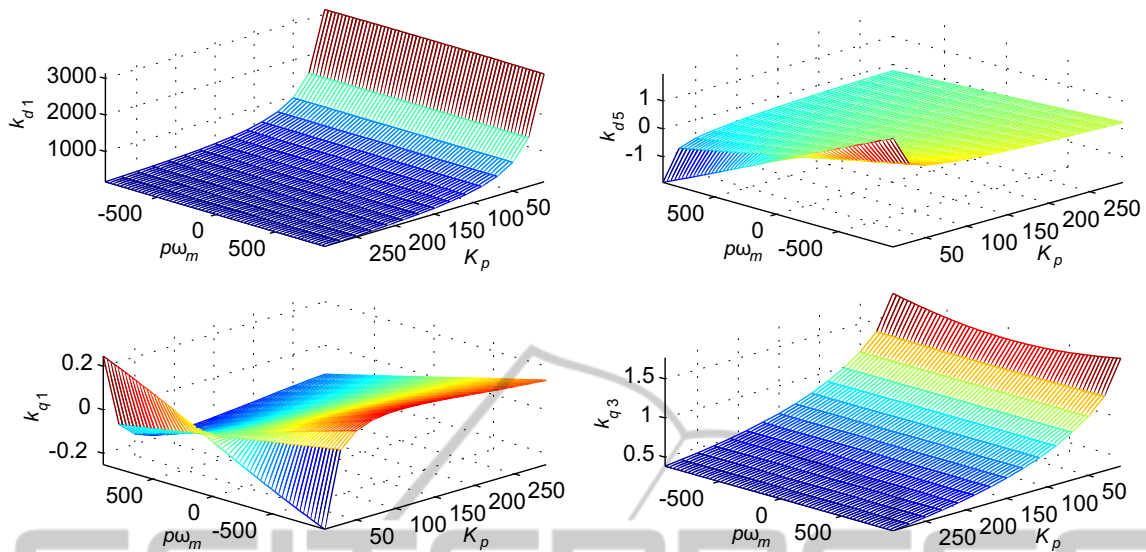
Figure 3: Examples of control gain surfaces.

- provide zero steady-state angular velocity error for step change of angular velocity reference and load torque step variations,

- achieve twice the rated current of PMSM ($i_{sn} = 5.8A$) during the step change of the reference angular velocity from 0 rad/s to $70\pi$ rad/s with the rated load torque ($T_{ln} = 8.8Nm$).

Assumptions presented above determine the maximum dynamics of the control system.

Table 2: Basic parameters of PMSM.

| Parameter | Value | Unit |
|-----------|-------|------|
| $P_N$ | 2.76 | kW |
| $R_s$ | 1.05 | $\Omega$ |
| $I_N$ | 5.8 | A |
| $L_s$ | 9.5 | mH |
| $T_{eN}$ | 8.8 | Nm |
| $K_t$ | 1.64 | Nm/A |
| $\Omega_{mN}$ | 314 | rad/s |
| $K_e$ | 98.84 | V/1000 |
| $B_m$ | $1.4 \times 10^{-3}$ | Nms/rad |
| $p$ | 3 | |
| $J_m$ | $6.2 \times 10^{-4}$ | kgm$^2$ |

For non-stationary system (7) with parameters given in table 2 and penalty matrices (10) ten non-linear control gain surfaces (CGS) have been constructed. Examples of CGS are presented in figure 3.

.

## 3.3 Artificial Neural Network Controller

Since it is difficult to find the analytical formulas that accurately approximate non-linear CGS described above, artificial neural network is employed in the proposed intelligent controller. Due to the learning and approximating capabilities of the ANNs (Ferrari and Stengel, 2005), (Huang and Tan, 2012), the designed neural network controller determines proper gain values (i.e. 10 coefficients) depend on operating point of the system.

It was found that CGS can be successfully approximated with the help of the feedforward back propagation neural network with 40 neurons in the first layer and 10 neurons in the output layer. Satisfactory level of the approximation (mean square error less than $1 \times 10^{-7}$) was achieved after 383 iterations. Sigmoidal functions were used as the activation functions in the first layer, while linear functions were used in the output layer.

## 3.4 Adaptation Algorithm

A simple adaptation algorithm presented in (Tarczewski et al., 2014) was used to determine an appropriate gain values of the buck converter and of the VSI. The reference value of the angular velocity $\omega_{mref}$ has been used as an input variable.

It was found that proper values of $K_{pvmc}$ and $K_{ppmsm}$ can be obtained when two low-pass filters with selector are used. The first one (2$^{nd}$ order low-pass with a cutoff frequency $f_{c1} = 20.8$Hz) is used to
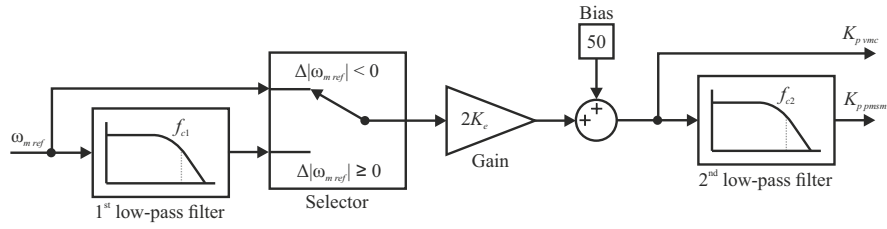
Figure 4: Block diagram of the adaptation algorithm.
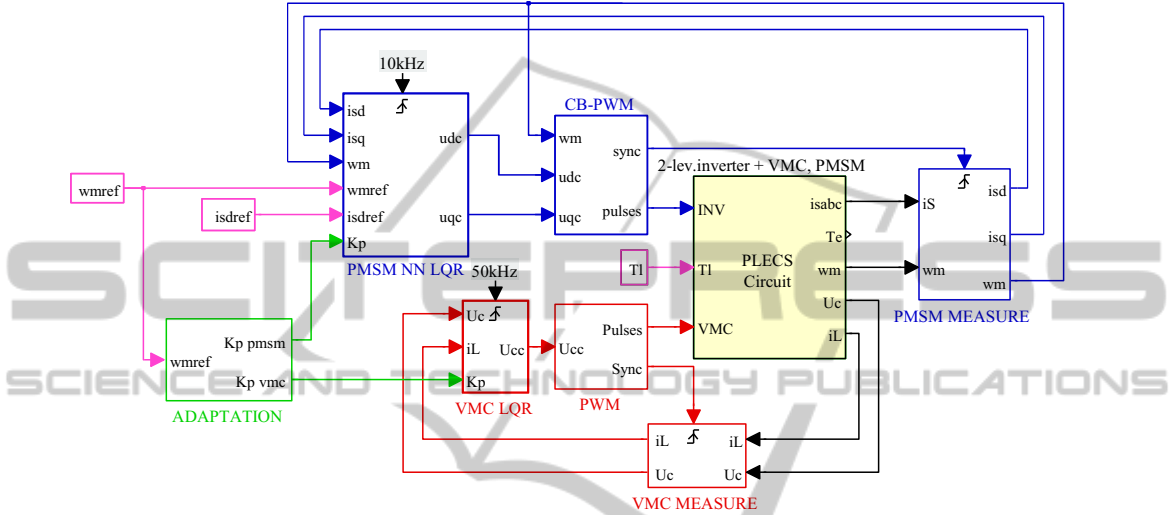


Figure 5: Schematic diagram of the proposed control structure.

calculate a reference value for VMC (figure 4). Introduced filter is used when absolute value of the reference velocity increases. Otherwise a reference value for VMC is calculated directly. An output gain of the filter was calculated from $K_e$ constant of the PMSM. A constant bias added to the output signal provides a sufficient gain of the inverter necessary to compensate rated load torque $T_{ln}$. The second filter ($2^{nd}$ order low pass with a cutoff frequency $f_{c2} = 128$Hz) is introduced to calculate an appropriate inverter's gain value $K_{p\,pmsm}$ for PMSM neural network controller.

The parameters of adaptation algorithm (i.e. $f_{c1}$, $f_{c2}$, Gain, Bias) presented above were determined empirically in order to provide torque ripple minimization and dynamic properties of the proposed control system similar to the typical one (i.e. PMSM fed by VSI).

## 4 SIMULATION RESULTS

Designed control system with neural network state feedback controller was implemented in a Matlab/Simulnik/Plecs environment (figure 5). In order to ensure proper generation of the control signals, designed state feedback controllers were imple-

mented in a triggered subsystems. The switching frequency of the VSI was set to $f_{s1} = 10$kHz, while the switching frequency of the buck converter was set to $f_{s2} = 50$kHz. Described in a previous section adaptation algorithm was implemented in an adaptation block. An additional triggered measure blocks were used to realize measurements in a midpoint of the PWM length. As a modulation technique typical carrier-based PWM has been used.

### 4.1 Dynamic Performances

Some selected results of dynamic tests are presented in figure 6. The angular velocity tracking performances of PMSM fed by VSI and by VMC + VSI for angular velocity reference changes: 10 rad/s, 90 rad/s, -40 rad/s are presented in figure 6.a and in figure 6.f respectively.

As it can be seen VMC doesn't deteriorate dynamics of the system. Designed neural network state feedback controller provides zero steady-state velocity error of PMSM and control strategy with zero $d$ axis current (figure 6.i). Waveforms of the electromagnetic torque produced by PMSM are shown in figure 6.b and in figure 6.g. From figure 6.h it can be seen, that proposed VMC properly maintain the level of the DC
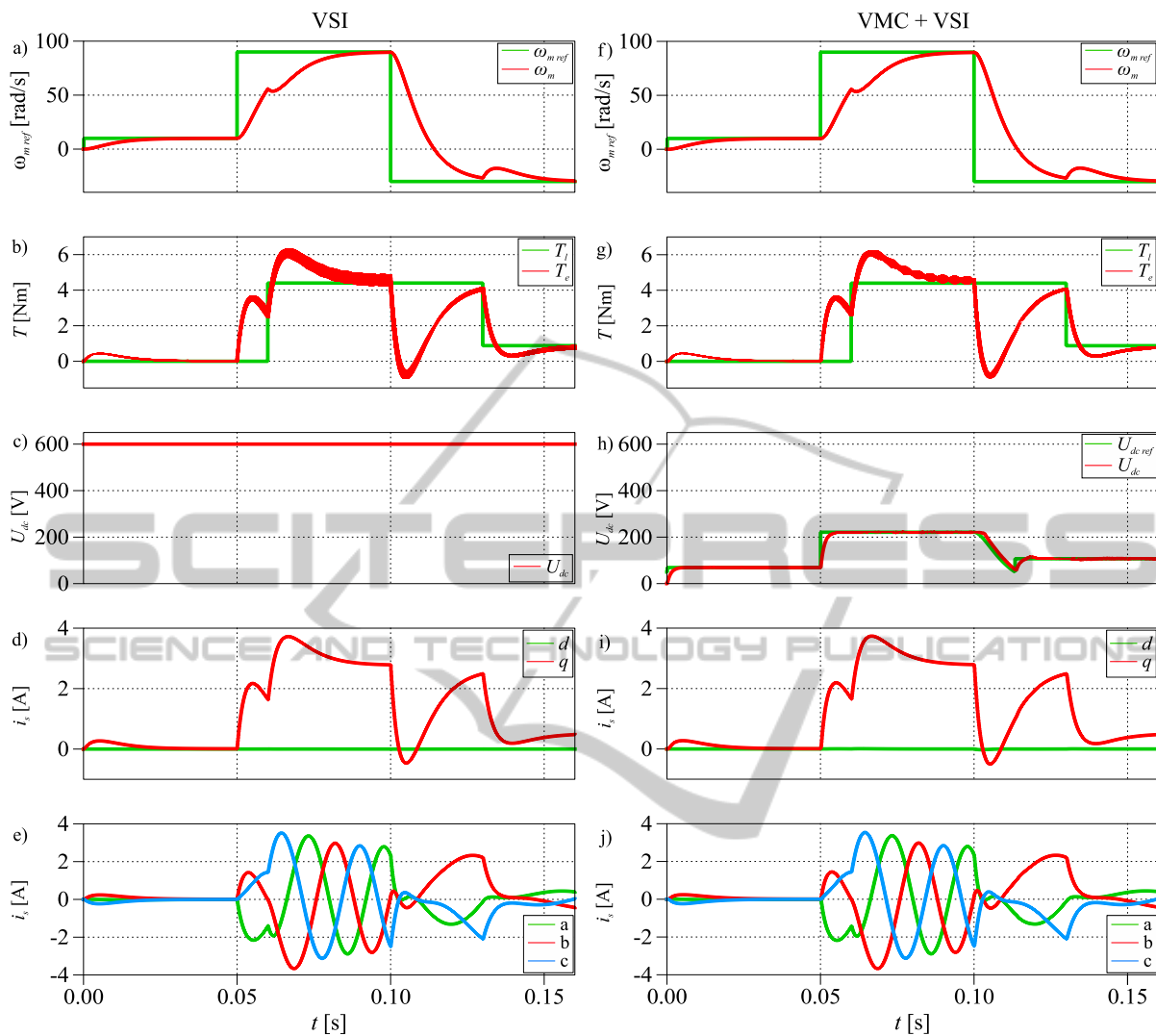
Figure 6: Simulation test results obtained for PMSM fed by: VSI - 1$^{st}$ column, VMC + VSI - 2$^{nd}$ column.

voltage demanded for PMSM operation under various conditions (i.e. angular velocity and load torque). Sinusoidal waveforms of PMSM phase currents are presented in figure 6.e and 6.j respectively.

## 4.2 Torque Ripple Analysis

Proposed control system with VMC and NN state feedback controller was examined in terms of PMSM torque ripple minimization. In order to evaluate the effectiveness of the proposed control system for torque ripple minimization, the torque ripple factor (*TRF*) was introduced (Qian et al., 2004):

$$TRF = \frac{T_{e\,pk-pk}}{T_{eN}} \times 100\% \qquad (11)$$

where: $T_{e\,pk-pk}$ - peak-to-peak torque ripple, $T_{eN}$ - rated torque of the PMSM.

Enlarged parts of the PMSM's electromagnetic torque waveforms observed for control systems (i.e. PMSM fed by VSI, PMSM fed by VMC + VSI) in a steady-state are shown in figure 7. Corresponding values of *TRF* are listed in table 3.

Table 3: Torque ripple factor.

| | $\omega_m$ [rad/s] | 10 | 50 | 100 |
|---|---|---|---|---|
| VSI | *TRF* [%] | 1.57 | 4.95 | 7.57 |
| VMC + VSI | *TRF* [%] | 1.21 | 2.06 | 2.04 |

From table 3 and figure 7 it can be seen that significant torque ripple minimization is achieved when proposed control system (i.e. VMC + VSI) is used.
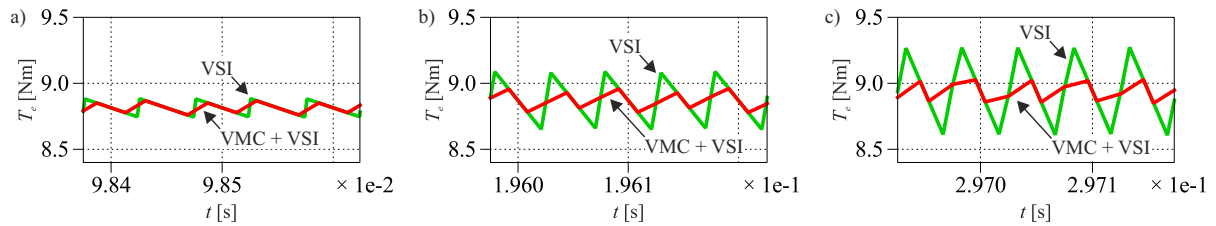
Figure 7: Electromagnetic torque waveforms of PMSM fed by VSI and VMC + VSI in a steady-state for the related load torque: a) $\omega_m = 10\text{rad/s}$, b) $\omega_m = 50\text{rad/s}$, c) $\omega_m = 100\text{rad/s}$.

## 5 CONCLUSIONS

It was found that neural network state feedback controller can be successfully used to control non-stationary and non-linear plant (i.e. PMSM fed by VSI with VMC) in terms of torque ripple minimization. Use of the proposed controller causes, that linearization and decoupling process of the plant are not needed. It was also found that DC voltage of the VSI can be precisely controlled with the help of an additional VMC control system.

Based on 2 low-order low-pass filters adaptive formula used to obtain an appropriate inverter gain with respect to actual value of the reference velocity was introduced.

Simulation test results confirm similar dynamic performance and significant torque ripple minimization of designed control system in comparison to PMSM fed by VSI with stationary state feedback controller - torque ripple factor is at least 30% smaller.

Experimental verification of the described control system with neural network based adaptive state feedback controller and voltage matching circuit is planned in the future.

## REFERENCES

Ferrari, S. and Stengel, R. F. (2005). Smooth function approximation using neural networks. *IEEE Transactions on Neural Networks*, 16(1):24–38.

Grzesiak, L. M. and Tarczewski, T. (2011). Permanent magnet synchronous motor discrete linear quadratic speed controller. In *IEEE International Symposium on Industrial Electronics, ISIE 2011*, pp. 667–672. IEEE.

Grzesiak, L. M. and Tarczewski, T. (2013). PMSM servo-drive control system with a state feedback and a load torque feedforward compensation. *COMPEL: The International Journal for Computation and Mathematics in Electrical and Electronic Engineering*, 32(1):364–382.

Gulez, K., Adam, A. A., and Pastaci, H. (2008). Torque ripple and EMI noise minimization in PMSM using active filter topology and field-oriented control. *IEEE Transactions on Industrial Electronics*, 55(1):251–257.

Hasanien, H. M. (2010). Torque ripple minimization of permanent magnet synchronous motor using digital observer controller. *Energy Conversion and Management*, 51(1):98–104.

Huang, S. and Tan, K. K. (2012). Intelligent friction modeling and compensation using neural network approximations. *IEEE Transactions on Industrial Electronics*, 59(8):3342–3349.

Hung, J. Y. and Ding, Z. (1993). Design of currents to reduce torque ripple in brushless permanent magnet motors. *IEE Proceedings B Electric Power Applications*, 140(4):260–266.

Jahns, T. M. and Soong, W. L. (1996). Pulsating torque minimization techniques for permanent magnet AC motor drives - a review. *IEEE Transactions on Industrial Electronics*, 43(2):321–330.

Kojima, M., Hirabayashi, K., Kawabata, Y., Ejiogu, E. C., and Kawabata, T. (2004). Novel vector control system using deadbeat-controlled PWM inverter with output LC filter. *IEEE Transactions on Industry Applications*, 40(1):162–169.

Krishnan, R. (2010). *Permanent Magnet Synchronous and Brushless DC Motor Drives*. CRC Press, New York.

Petrovic, V., Ortega, R., Stankovic, A. M., and Tadmor, G. (2000). Design and implementation of an adaptive controller for torque ripple minimization in PM synchronous motors. *IEEE Transactions on Power Electronics*, 15(5):871–880.

Qian, W., Panda, S. K., and Xu, J.-X. (2004). Torque ripple minimization in PM synchronous motors using iterative learning control. *IEEE Transactions on Power Electronics*, 19(2):272–279.

Steinke, J. K. (1999). Use of an LC filter to achieve a motor-friendly performance of the PWM voltage source inverter. *IEEE Transactions on Energy Conversion*, 14(3):649–654.

Tarczewski, T. and Grzesiak, L. M. (2013). PMSM fed by 3-level NPC sinusoidal inverter with discrete state feedback controller. In *15th European Conference on Power Electronics and Applications, EPE 2013*, pp. 1–9. IEEE.

Tarczewski, T., Niewiara, L., and Grzesiak, L. M. (2014). Torque ripple minimization for PMSM using voltage matching circuit and neural network based adaptive state feedback control. In *16th European Conference on Power Electronics and Applications, EPE 2014*. IEEE.

Tewari, A. (2002). *Modern Control Design: with MATLAB and SIMULINK*. Wiley, Chichester.